

Spin-orbit coupling controlled ground state in $\text{Sr}_2\text{ScOsO}_6$

A. E. Taylor,¹ R. Morrow,² R. S. Fishman,³ S. Calder,¹ A.I. Kolesnikov,⁴
M. D. Lumsden,¹ P. M. Woodward,² and A. D. Christianson^{1,5}

¹Quantum Condensed Matter Division, Oak Ridge National Laboratory, Oak Ridge, Tennessee 37831, USA

²Department of Chemistry, The Ohio State University, Columbus, Ohio 43210-1185, USA

³Materials Science and Technology Division, Oak Ridge National Laboratory, Oak Ridge, Tennessee 37831, USA

⁴Chemical and Engineering Materials Division, Oak Ridge National Laboratory, Oak Ridge, Tennessee 37831, USA

⁵Department of Physics and Astronomy, The University of Tennessee, Knoxville, TN 37996, USA

We report neutron scattering experiments which reveal a large spin gap in the magnetic excitation spectrum of weakly-monoclinic double perovskite $\text{Sr}_2\text{ScOsO}_6$. The spin gap is demonstrative of appreciable spin-orbit-induced anisotropy, despite nominally orbitally-quenched $5d^3$ Os^{5+} ions. The system is successfully modeled including nearest neighbor interactions in a Heisenberg Hamiltonian with exchange anisotropy. We find that the presence of the spin-orbit-induced anisotropy is essential for the realization of the type I antiferromagnetic ground state. This demonstrates that physics beyond the LS or JJ coupling limits plays an active role in determining the collective properties of $4d^3$ and $5d^3$ systems, and that theoretical treatments must include spin-orbit coupling.

PACS numbers: 71.70.Ej, 71.70.Gm, 78.70.Nx

The role of spin-orbit coupling (SOC) in $4d$ and $5d$ transition metal oxides is relatively poorly understood outside of the *LS* and *JJ* coupling limits. The need to understand the intermediate regime is typified by the diverse range of properties found in double perovskites (DPs) containing $4d$ and $5d$ ions, including high-temperature half-metallic ferrimagnetism [1, 2], structurally selective magnetic states [3–5], complex geometric frustration [6–11], and Mott insulating states [12–14]. Whilst the complex array of ground states has generated a great deal of interest, the interaction mechanisms controlling them remain undetermined.

For DPs hosting $4d^3$ or $5d^3$ ions, the role of SOC is particularly unclear. There exists dispute between different theories describing SOC and its influence on the interactions [10, 14–20]. To first order, d^3 ions in an octahedral environment are expected to be orbitally quenched, Fig. 1(a) [9, 17], yet there is mounting evidence that SOC has considerable influence [6, 11, 21–23]. This has been demonstrated by the presence of ~ 2 – 18 meV gaps in the magnetic excitation spectra of Ba_2YRuO_6 , $\text{La}_2\text{NaRuO}_6$ and Ba_2YO_6 [9, 11, 21]. Such large gaps, on the same energy scale as the T_N s, implies a departure from an orbital singlet, and raises the question of how SOC manifests in the collective properties.

Beyond a fundamental interest in the influence of SOC, it is vital to determine the sign and strength of exchange interactions between $5d$ ions in order to understand the magnetism of many DPs, including the exceptionally high $T_C = 725$ K seen in $\text{Sr}_2\text{CrOsO}_6$ [24, 25]. Investigations of $\text{Sr}_2\text{CrOsO}_6$ and related materials show that exchange interactions between Os^{5+} ions cannot be neglected [3, 14, 18–20, 23, 26]. However, the strong coupling between Cr^{3+} and Os^{5+} ions makes it difficult to measure the strength of the Os-Os coupling. Additionally, there is a lack of agreement regarding the mecha-

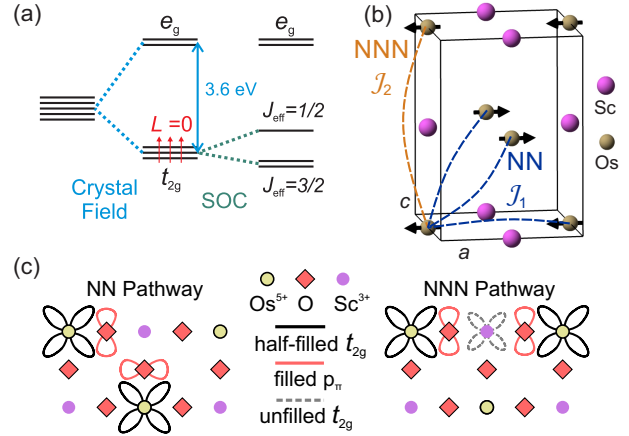


Figure 1. (a) Schematic of the energy levels for Os^{5+} in an octahedral environment. t_{2g} - e_g splitting of 3.6 eV determined by x-ray absorption spectroscopy [30]. In the strong SOC limit the t_{2g} level can be further split into $J_{\text{eff}} = \frac{1}{2}$ and $\frac{3}{2}$ levels. Nominally the Os^{5+} ion is in the *LS* coupling limit and an $L = 0$ state results. (b) $\text{Sr}_2\text{ScOsO}_6$ magnetic structure, with moments depicted along a . One $P2_1/n$ unit cell is shown, with O and Sr ions omitted for clarity. Dashed lines show examples of the NN ($\times 12$) \mathcal{J}_1 and NNN ($\times 6$) \mathcal{J}_2 exchanges. (c) Schematic of the relevant orbitals for NN and NNN exchange pathways, assuming formal valence states.

nism that stabilizes type I antiferromagnetic (AFM) order on the face-centered-cubic (FCC) lattice of B' ions in $A_2BB'O_6$ DPs, where B is diamagnetic, and B' is either Ru^{5+} ($4d^3$) or Os^{5+} ($5d^3$) [10, 11]. Most attempts to determine the exchange interactions in these systems have been limited to theoretical models not directly related to measurements, with conflicting results [10, 14, 27–29]. Therefore, to understand the underlying behavior, it is desirable to obtain the interactions experimentally.

To access Os^{5+} ion interactions experimentally, we in-

investigate $\text{Sr}_2\text{ScOsO}_6$. It is the single-magnetic-ion analogue of $\text{Sr}_2\text{CrOsO}_6$, therefore all magnetic interactions result solely from the frustrated quasi-FCC Os^{5+} lattice. Despite this, $\text{Sr}_2\text{ScOsO}_6$ hosts a remarkably high T_N (92 K) for a single-magnetic-ion DP [23, 31, 32]. It is therefore a model system for investigating the role of the $\text{Os}^{5+} 5d^3$ magnetic interactions in a high transition temperature material.

We present the inelastic neutron scattering (INS) spectrum of $\text{Sr}_2\text{ScOsO}_6$, and find a large spin gap below T_N . A Heisenberg Hamiltonian with anisotropic exchange terms is considered. We find that over a large parameter space, the solution which best describes the data is one with the isotropic nearest-neighbor (NN) term $J_1 = -4.4$ meV, and negligible next-nearest-neighbor (NNN) interactions. The success of the model reveals that anisotropy is essential to selection of the type I AFM ground state. This suggests that SOC within the $5d^3$ manifold, along with strong Os-O hybridization, promotes a high T_N in this otherwise frustrated material. Therefore, it is NN interactions combined with SOC-induced anisotropy that are key to the collective behavior realized in $\text{Sr}_2\text{ScOsO}_6$, and related $4d^3$ and $5d^3$ systems. This demonstrates that SOC must be included in theoretical treatments of these materials.

A 16.5 g polycrystalline sample of $\text{Sr}_2\text{ScOsO}_6$ was used for INS experiments on SEQUOIA at the Spallation Neutron Source at Oak Ridge National Laboratory [33], see Supplemental Material (SM) [34] for full details. The structural and magnetic properties of the same sample were reported in Ref. [23], finding space group $P2_1/n$ with $a = 5.6398(2)$ Å, $b = 5.6373(2)$ Å, $c = 7.9884(3)$ Å and $\beta = 90.219(2)^\circ$ at 5 K, and $T_N = 92$ K.

Measured INS spectra are shown in Fig. 2. There is a pronounced change in the spectrum at low neutron momentum transfer (Q) upon crossing T_N . This behavior is reminiscent of the observed gap development below T_N in other single magnetic ion $4d^3$ and $5d^3$ DPs [9, 11, 21]. The higher Q scattering, which changes only in intensity with temperature, is identified as phonon scattering.

The detailed (Q, E) -space structure and temperature dependence of the scattering is presented in Fig. 3. Figure 3(a) demonstrates that intensity is distributed to higher energies at low temperatures, as expected from a gap opening. The peak of the scattering intensity at 6 K is at $\eta = 19(2)$ meV. This compares to previous observations, which have been used as a magnitude estimate for the gap, of $\eta = 18(2)$ meV in Ba_2YOsO_6 ($T_N=69$ K), $\eta \approx 5$ meV in Ba_2YRuO_6 ($T_N=36$ K) and $\eta \approx 2.75$ meV in $\text{La}_2\text{NaRuO}_6$ ($T_N=15$ K) [9, 11, 21]. This generally supports a picture of gap energy scale varying with T_N . Figure 3(c) presents data that has been corrected for the Bose thermal population factor, $[1 - \exp(-E/k_B T)]^{-1}$. The sharp drop in intensity at low E below T_N demonstrates the opening of the gap.

Constant- E cuts averaged from 5 to 9 meV show

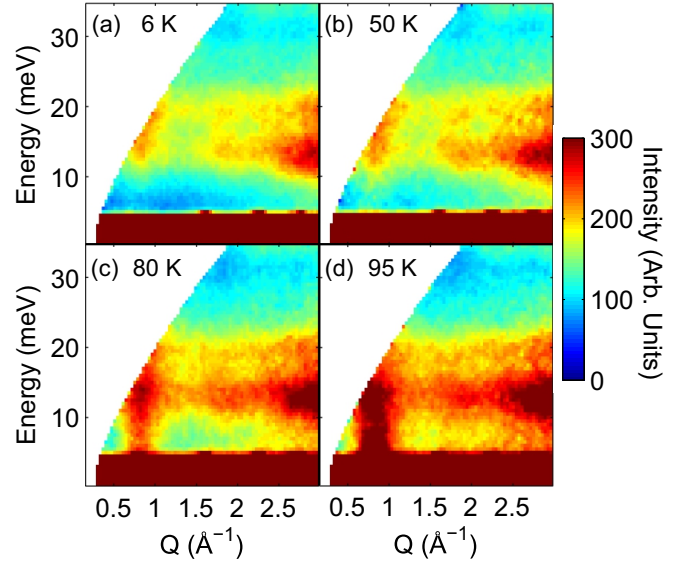


Figure 2. $E_i = 60$ meV neutron scattering intensity maps for $95 \text{ K} \approx T_N$, and $T < T_N$ of 80, 50 and 6 K.

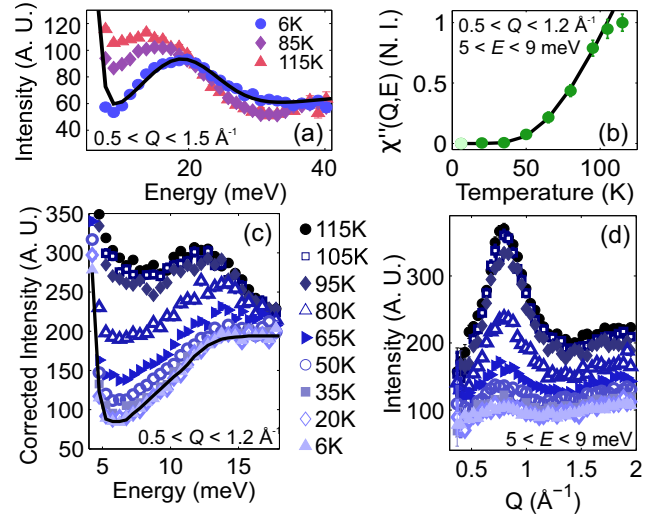


Figure 3. (a) Constant- Q cuts from $E_i = 120$ meV data. Solid line is the result of fitting Gaussians to the elastic line and to the inelastic magnetic signal at 6 K. A. U. stands for arbitrary units. (b) $\chi''(T)$ at fixed Q and E , with an exponential, $\chi''(T) \propto \exp(-\Delta/k_B T)$, fit to the $T < T_N$ data. N.I. stands for normalized intensity. (c) Constant- Q cuts from $E_i = 60$ meV data, which have been corrected for the Bose factor. Solid line is a guide to the eye. (d) Constant- E cuts from $E_i = 60$ meV data. In all panels, errorbars are sometimes smaller than the symbols.

scattering centered around AFM ordering wavevector $|\mathbf{Q}_{(001)}| \approx 0.8 \text{ Å}^{-1}$, Fig. 3(d), with some asymmetry in the lineshape resulting from $|\mathbf{Q}_{(100)/(010)}| \approx 1.1 \text{ Å}^{-1}$ fluctuations. To track the relative strength of the fluctuations we extract the dynamic susceptibility, $\chi''(T)$, for fixed range $5 < E < 9$ meV and $0.5 < Q < 1.2 \text{ Å}^{-1}$ via

the same method as Ref. [11] (see also SM [34]). The opening of a gap below T_N is again indicated, Fig. 3(b), by the reduction in $\chi''(T)$ evaluated at low-energy.

We investigate a model Heisenberg Hamiltonian with anisotropic exchange terms. The results we present here include only NN terms, \mathcal{J}_1 , (see Fig. 1(b)) because the NNN terms, \mathcal{J}_2 , are dramatically suppressed (estimated as $J_2 \leq 0.01J_1$ in Ref. [10]), as discussed below. We tested this assumption by seeking solutions over a wide range of parameter space with $\mathcal{J}_2 \neq 0$, see SM [34], but found that $\mathcal{J}_2 = 0$ provided the best description of the experimental INS data.

The model is parametrized with an isotropic term, J_1 , which is decoupled from the physical origin of the spin gap, and an exchange anisotropy term, K_1 , to account for the gap. Unlike isotropic exchange terms, anisotropic exchange terms only couple to a particular component of spin, e.g. S_x . x represents the direction of spin alignment. We assume that the exchange interactions are unaffected by the weak monoclinic distortion, justified by two considerations: first, the distortion is much smaller than found in d^3 systems in which the distortion is reported to affect the physical properties [6, 34, 35]. Secondly, the properties of the closely related cubic compound Ba_2YOsO_6 are remarkably similar to $\text{Sr}_2\text{ScOsO}_6$ [11]. The Hamiltonian is therefore

$$\mathcal{H} = - \sum_{\text{NN}} \mathcal{J}_1^{\alpha\beta} S_{i\alpha} S_{j\beta} = - \sum_{\text{NN}} (J_1 \mathbf{S}_i \cdot \mathbf{S}_j + K_1 S_{ix} S_{jx}).$$

J_1 and K_1 are defined such that positive values are ferromagnetic (FM) and negative values are AFM. The exchange parameters scale inversely with spin, with $s = 0.8$ determined from neutron diffraction [23] [36].

To accurately reproduce the INS data from $\text{Sr}_2\text{ScOsO}_6$, we use the bottom and top of the spin wave band, $\Delta = 12$ meV and $\Gamma = 40$ meV, respectively, as conditions to determine the parameters J_1 and K_1 . Δ was determined by inspection of the 6 K data in Fig. 3(c), in which the increasing intensity begins to saturate at $E \approx 12$ meV. Γ was determined by inspection of broad constant- Q cuts from the $E_i = 120$ meV data (see SM Fig. S2 [34]), designed to capture all magnetic scattering up to high energies, in which 6 K and 115 K cuts converge at 40 meV. An additional constraint for the local stability of the ground state, depicted in Fig. 1(b), is that the spin-wave frequencies are real throughout the magnetic Brillouin zone. Utilizing this model, we find the solution $J_1 = -4.4$ meV and $K_1 = -3.8$ meV. This gives a mean-field transition temperature of 181 K, two times greater than the measured T_N . This is reasonable, as calculated mean-field temperatures are generally expected to exceed measured values [37], and the Curie-Weiss constant for this compound, $\Theta = -677$ K [23], is also far greater than $T_N = 92$ K.

The simulated powder-averaged INS cross section $S(Q, E)$ for $J_1 = -4.4$ meV and $K_1 = -3.8$ meV is com-

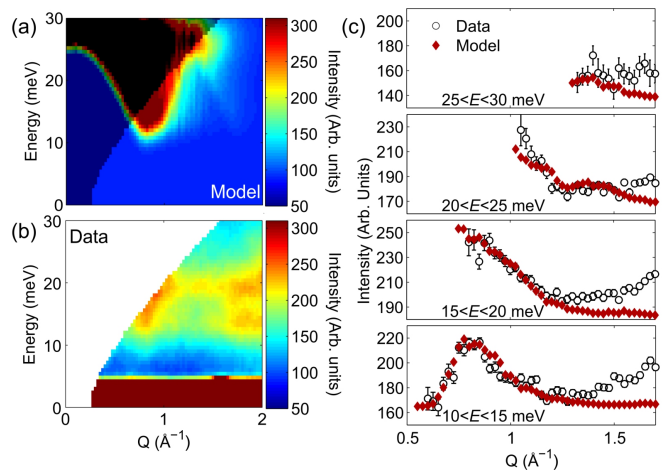


Figure 4. (a) Simulated spin-wave spectra. Modeled using linear spin-wave theory [38], with powder averaging performed by sampling 10^4 random points in reciprocal space. Gaussian energy broadening of 4 meV is applied as an approximation to instrument resolution at $E_i = 60$ meV, estimated from the full width at half maximum of the incoherent part of the elastic line in the data. (b) The equivalent data collected at $T = 6$ K. The intensity at high Q in the data is due to phonon scattering, which is not included in the model. The shaded region in the calculations indicates the region of (Q, E) space which is inaccessible in the experiment. (c) Constant-energy cuts through the calculation and data. A global scale factor has been used for the calculation, and a flat background applied for each cut.

pared to the low-temperature data in Fig. 4, and we find good agreement. An overview is provided by colormaps in Fig. 4(a) and (b), and a more detailed comparison is given by constant-energy cuts in Fig. 4(c). Note that this solution is equivalent to a single-ion anisotropy model with $J_1 = -4.4$ meV and $D = 7.5$ meV.

Although SOC has been noted as the origin of the spin gap in $5d$ DPs [11, 21], the underlying mechanism by which it acts to produce the gap remains an open question. In general, the possible mechanisms in a three dimensional system are Dzyaloshinsky-Moriya (DM) interactions, single-ion anisotropy, and exchange anisotropy, all of which are induced by SOC. There are two observations which favor dismissal of the DM interaction as the origin of the gap: (i) the highly symmetric cubic or close-to-cubic crystal structures in which the gap has been observed (space group $Fm\bar{3}m$ has inversion symmetry at the Os site, $P2_1/n$ does not) and (ii) the type I collinear AFM structure common to several DPs including $\text{Sr}_2\text{ScOsO}_6$ – two perpendicular DM interactions would be required to produce a gap, but would favor a non-collinear spin state.

We also expect that single-ion anisotropy is negligible, because it is dramatically suppressed for the orbitally suppressed d^3 configuration, and the 3.6 eV t_{2g} to e_g splitting in $\text{Sr}_2\text{ScOsO}_6$ [30] means that the excited

state perturbations are minimal [39]. This is supported by the experimental observation that no gap emerges in $\text{La}_2\text{NaOsO}_6$ which only displays short-range order, whereas a gap is observed in long-ranged-ordered sister-compound $\text{La}_2\text{NaRuO}_6$ [21]. A single-ion term, being a local effect, would not be sensitive to short- versus long-range order, and would emerge in the short-range ordered state. Therefore, exchange anisotropy is the most-likely explanation for the gap in $4d^3$ and $5d^3$ DPs. Independent of the gap's origin, the determination that $J_1 \approx -4.4$ meV and J_2 is negligibly small, has significant consequences.

There is dispute in the literature over the strength of long-range interactions in d^3 DPs, and the origin of type I AFM order in $4d$ and $5d$ single-magnetic-ion DPs. Competition between type I and type III order results in frustration on the (quasi)-FCC lattice of Os/Ru ions. Theoretical studies found that type I order can be stabilized either by a FM J_2 in an isotropic (i.e. $K_1 = 0$) Heisenberg Hamiltonian, or by some form of anisotropy [10]. Nilsen *et al.* [22] attempted to extract the interactions in Ba_2YRuO_6 via Reverse Monte Carlo (RMC) analysis of diffuse neutron scattering, and found large interactions beyond NN, with $|J_2| \approx \frac{1}{2}|J_1|$. However, by use of an isotropic Heisenberg Hamiltonian, their analysis implicitly assumed significant long-range interactions to stabilize the correct ground state, and, as they point out, could not distinguish from an anisotropy-based model. We have found that, in-fact, an NN-only exchange model with significant SOC-induced anisotropy provides the best description of the INS spectrum for $\text{Sr}_2\text{ScOsO}_6$.

Our result can be rationalized based on the superexchange pathways present, illustrated in Fig. 1(c). The NN Os-O-O-Os superexchange pathway is anticipated to be strongly AFM due to the half-filled Os^{5+} t_{2g} levels [40, 41]. Direct t_{2g} - t_{2g} overlap is also an AFM NN contribution. The NNN pathway, however, relies on overlap with empty Sc^{3+} t_{2g} orbitals, and was estimated as $J_2 \leq 0.01J_1$ in Ref. [10], consistent with our result.

This analysis is, however, at odds with attempts to model the exchange interactions in $3d^x$ - $5d^3$ DPs, including $\text{Sr}_2\text{CrOsO}_6$, using density functional theory [18, 27–29]. Studies estimated $|J_2|$ in the range 1.9–24 meV (for $s = 0.8$ meV), but did not consider the anisotropy terms (single-ion or exchange anisotropy) reported here, despite mentioning the likely frustration of Os^{5+} ions. Therefore, much like the modeling of Ba_2YRuO_6 via RMC, the longer-range interactions may have been implicitly forced to have large values. This is particularly relevant in $\text{Sr}_2\text{CrOsO}_6$, in which both magnetic ions have d^3 configuration, therefore unlike $(\text{Ca},\text{Sr})_2\text{FeOsO}_6$ no occupied e_g orbital pathways contribute to longer-range interactions [4, 42]. Anisotropy could therefore have a major influence in $\text{Sr}_2\text{CrOsO}_6$, and further calculations including anisotropy terms would be illuminating. Similar calculations for $\text{Sr}_2\text{ScOsO}_6$ will be directly constrained by the

size of the observed gap and by $J_1 \approx -4.4$ meV, independent of the gap's origin.

As anisotropy is essential in stabilizing the AFM order in $\text{Sr}_2\text{ScOsO}_6$, it should also be relevant in type I Ba_2YOsO_6 , Ba_2YRuO_6 and Sr_2YRuO_6 [7, 11, 43, 44]. Diffraction experiments found no structural distortion (Ba_2YOsO_6 and Ba_2YRuO_6), or a small monoclinic distortion (Sr_2YRuO_6), therefore the same interaction pathways as for $\text{Sr}_2\text{ScOsO}_6$ are applicable. Although exchange/single-ion anisotropies are formally absent (to 2nd order) in a cubic system [39], the type I order should coincide with a distortion via magneto-elastic coupling in Ba_2YOsO_6 and Ba_2YRuO_6 . Although this structural distortion, if present, is outside the range of detection of present diffraction experiments, it would allow anisotropy to enter the Hamiltonian. Anisotropy has been directly observed via spin-gaps in both these materials [9, 11]. We therefore propose that in all these systems, SOC is essential in determining the magnetic ground state.

Amongst these materials, $\text{Sr}_2\text{ScOsO}_6$ boasts the highest T_N . As has previously been noted, large Os-O hybridization is an important factor in heightened T_N s [18, 23]. Our results suggest that, by promoting selection of a particular ground state and relieving frustration, Os^{5+} SOC also acts to enhance T_N in $\text{Sr}_2\text{ScOsO}_6$. This notion is supported by the trend in gap size with T_N across the measured compounds, and by the observation that $3d$ transition metal DPs have lower T_N s and usually favor a different, Type II, ground state [45].

It is also informative to compare $\text{Sr}_2\text{ScOsO}_6$ to the equivalent $5d^2$ systems $\text{Sr}_2\text{MgOsO}_6$ [32] and $\text{Sr}_2\text{ScReO}_6$ [46, 47]. We expect $5d^2$ ions to have a smaller magnetic moment [48], and reduced Os-O-O-Os AFM superexchange as the t_{2g} levels are not half-filled. This results in a lower AFM energy scale, but unquenched SOC, which will promote a high T_N compared to that AFM energy scale if the SOC promotion of T_N is correct. Both these expectations are met - compared to $\text{Sr}_2\text{ScOsO}_6$ these compounds have lower inherent energy scales as indicated by their Curie Weiss constants, but have T_N s of 105 K and 75 K, comparable to that of $\text{Sr}_2\text{ScOsO}_6$. Therefore SOC has an important role in high- T_N DPs beyond the $5d^3$ case.

In conclusion, by modeling the magnetic excitation spectrum of archetypal system $\text{Sr}_2\text{ScOsO}_6$, we have extracted the exchange parameters resulting from Os^{5+} ion interactions. The presence of a large spin gap demonstrates that SOC is significant, i.e. the $5d^3$ ions deviate from the nominal orbital singlet expected from LS coupling. We find that only NN interactions are significant, and as a consequence, SOC-induced anisotropy governs the magnetic state in this otherwise frustrated system, and assists in promoting a high T_N . This demonstrates that the interplay of NN interactions with anisotropy should be considered for the collective properties of high- T_C $5d^3$ systems, particularly $\text{Sr}_2\text{CrOsO}_6$.

The authors gratefully acknowledge M. B. Stone, S. E. Nagler and B. D. Gaulin for useful discussions. The research at Oak Ridge National Laboratory's Spallation Neutron Source was supported by the Scientific User Facilities Division, Office of Basic Energy Sciences, U.S. Department of Energy (DOE). Support for a portion of this research was provided by the Center for Emergent Materials an NSF Materials Research Science and Engineering Center (DMR-1420451). Research by RF sponsored by the DOE, Office of Science, Basic Energy Sciences, Materials Sciences and Engineering Division.

This manuscript has been authored by UT-Battelle, LLC under Contract No. DE-AC05-00OR22725 with the U.S. Department of Energy. The United States Government retains and the publisher, by accepting the article for publication, acknowledges that the United States Government retains a non-exclusive, paid-up, irrevocable, world-wide license to publish or reproduce the published form of this manuscript, or allow others to do so, for United States Government purposes. The Department of Energy will provide public access to these results of federally sponsored research in accordance with the DOE Public Access Plan (<http://energy.gov/downloads/doe-public-access-plan>).

-
- [1] K.-I. Kobayashi, T. Kimura, H. Sawada, K. Terakura, and Y. Tokura, *Nature* **395**, 677 (1998).
 - [2] K.-I. Kobayashi, T. Kimura, Y. Tomioka, H. Sawada, K. Terakura, and Y. Tokura, *Phys. Rev. B* **59**, 11159 (1999).
 - [3] H. L. Feng, M. Arai, Y. Matsushita, Y. Tsujimoto, Y. Guo, C. I. Sathish, X. Wang, Y.-H. Yuan, M. Tanaka, and K. Yamaura, *J. Am. Chem. Soc.* (2014).
 - [4] R. Morrow, J. W. Freeland, and P. M. Woodward, *Inorg. Chem.* **53**, 7983 (2014).
 - [5] R. Morrow, J. Yan, M. A. McGuire, J. W. Freeland, D. Haskell, and P. M. Woodward, *Phys. Rev. B* **92**, 094435 (2015).
 - [6] A. A. Aczel, D. E. Bugaris, L. Li, J.-Q. Yan, C. de la Cruz, H.-C. zur Loye, and S. E. Nagler, *Phys. Rev. B* **87**, 014435 (2013).
 - [7] T. Aharen, J. E. Greedan, F. Ning, T. Imai, V. Michaelis, S. Kroeker, H. Zhou, C. R. Wiebe, and L. M. D. Cran-
swick, *Phys. Rev. B* **80**, 134423 (2009).
 - [8] P. L. Bernardo, L. Ghivelder, H. S. Amorim, J. J. Neumeier, and S. Garcia, *arXiv:1509.04377* (2015).
 - [9] J. P. Carlo, J. P. Clancy, K. Fritsch, C. A. Marjerrison, G. E. Granroth, J. E. Greedan, H. A. Dabkowska, and B. D. Gaulin, *Phys. Rev. B* **88**, 024418 (2013).
 - [10] E. V. Kuz'min, S. G. Ovchinnikov, and D. J. Singh, *Phys. Rev. B* **68**, 024409 (2003).
 - [11] E. Kermarrec, C. A. Marjerrison, C. M. Thompson, D. D. Maharaj, K. Levin, S. Kroeker, G. E. Granroth, R. Flacau, Z. Yamani, J. E. Greedan, and B. D. Gaulin, *Phys. Rev. B* **91**, 075133 (2015).
 - [12] A. S. Erickson, S. Misra, G. J. Miller, R. R. Gupta, Z. Schlesinger, W. A. Harrison, J. M. Kim, and I. R. Fisher, *Phys. Rev. Lett.* **99**, 016404 (2007).
 - [13] S. Gangopadhyay and W. E. Pickett, *Phys. Rev. B* **91**, 045133 (2015).
 - [14] O. N. Meetei, O. Erten, M. Randeria, N. Trivedi, and P. Woodward, *Phys. Rev. Lett.* **110**, 087203 (2013).
 - [15] S. Middey, A. K. Nandy, S. K. Pandey, P. Mahadevan, and D. D. Sarma, *Phys. Rev. B* **86**, 104406 (2012).
 - [16] H. Matsuura and K. Miyake, *J. Phys. Soc. Jpn.* **82**, 073703 (2013).
 - [17] G. Chen and L. Balents, *Phys. Rev. B* **84**, 094420 (2011).
 - [18] H. Das, P. Sanyal, T. Saha-Dasgupta, and D. D. Sarma, *Phys. Rev. B* **83**, 104418 (2011).
 - [19] P. Sanyal, *Phys. Rev. B* **89**, 115129 (2014).
 - [20] K. Samanta, P. Sanyal, and T. Saha-Dasgupta, *Scientific Reports* **5**, 15010 (2015).
 - [21] A. A. Aczel, P. J. Baker, D. E. Bugaris, J. Yeon, H.-C. zur Loye, T. Guidi, and D. T. Adroja, *Phys. Rev. Lett.* **112**, 117603 (2014).
 - [22] G. J. Nilsen, C. M. Thompson, G. Ehlers, C. A. Marjerrison, and J. E. Greedan, *Phys. Rev. B* **91**, 054415 (2015).
 - [23] A. E. Taylor, R. Morrow, D. J. Singh, S. Calder, M. D. Lumsden, P. M. Woodward, and A. D. Christianson, *Phys. Rev. B* **91**, 100406 (2015).
 - [24] Y. Krockenberger, M. Reehuis, M. Tovar, K. Mogare, M. Jansen, and L. Alff, *Journal of Magnetism and Magnetic Materials* **310**, 1854 (2007).
 - [25] Y. Krockenberger, K. Mogare, M. Reehuis, M. Tovar, M. Jansen, G. Vaitheeswaran, V. Kanchana, F. Bultmark, A. Delin, F. Wilhelm, A. Rogalev, A. Winkler, and L. Alff, *Phys. Rev. B* **75**, 020404 (2007).
 - [26] A. K. Paul, M. Reehuis, V. Ksenofontov, B. Yan, A. Hoser, D. M. Többens, P. M. Abdala, P. Adler, M. Jansen, and C. Felser, *Phys. Rev. Lett.* **111**, 167205 (2013).
 - [27] S. Kanungo, B. Yan, M. Jansen, and C. Felser, *Phys. Rev. B* **89**, 214414 (2014).
 - [28] Y. S. Hou, H. J. Xiang, and X. G. Gong, *Scientific Reports* **5**, 13159 (2015).
 - [29] J. Wang, N. Zu, X. Hao, Y. Xu, Z. Li, Z. Wu, and F. Gao, *Physica Status Solidi (RRL)* **08**, 776 (2014).
 - [30] J.-H. Choy, D.-K. Kim, and J.-Y. Kim, *Solid State Ionics* **108**, 159 (1998).
 - [31] A. K. Paul, A. Sarapulova, P. Adler, M. Reehuis, S. Kanungo, D. Mikhailova, W. Schnelle, Z. Hu, C. Kuo, V. Siruguri, S. Rayaprol, Y. Soo, B. Yan, C. Felser, L. Hao Tjeng, and M. Jansen, *Z. anorg. allg. Chem.* **641**, 197 (2015).
 - [32] Y. Yuan, H. L. Feng, M. P. Ghimire, Y. Matsushita, Y. Tsujimoto, J. He, M. Tanaka, Y. Katsuya, and K. Yamaura, *Inorg. Chem.* **54**, 3422 (2015).
 - [33] G. E. Granroth, A. I. Kolesnikov, T. E. Sherline, J. P. Clancy, K. A. Ross, J. P. C. Ruff, B. D. Gaulin, and S. E. Nagler, *J. Phys.: Conf. Ser.* **251**, 012058 (2010).
 - [34] Supplementary material includes additional experimental details, INS data and spin-wave model calculations.
 - [35] M. Retuerto, M. García-Hernández, M. J. Martínez-Lope, M. T. Fernández-Díaz, J. P. Attfield, and J. A. Alonso, *J. Mater. Chem.* **17**, 3555 (2007).
 - [36] From $m = 1.6(1) \mu_B$ assuming a g-factor of 2, deemed reasonable since density functional theory finds the ratio of spin to orbital moments is ~ 15 [23].
 - [37] D. C. Mattis, *The Theory of Magnetism* (Harper & Row, New York, 1965).

- [38] S. Toth and B. Lake, J. Phys.: Condens. Matter **27**, 166002 (2015).
- [39] D. I. Khomskii, *Transition Metal Compounds*, 1st ed. (Cambridge University Press, Cambridge, 2014).
- [40] J. B. Goodenough, Phys. Rev. **100**, 564 (1955).
- [41] J. Kanamori, J. Phys. Chem. Solids **10**, 87 (1959).
- [42] L. S. I. Veiga, G. Fabbri, M. van Veenendaal, N. M. Souza-Neto, H. L. Feng, K. Yamaura, and D. Haskel, Phys. Rev. B **91**, 235135 (2015).
- [43] P. Battle and C. Jones, J. Solid State Chem. **78**, 108 (1989).
- [44] P. Battle and W. Macklin, J. Solid State Chem. **52**, 138 (1984).
- [45] S. Vasala and M. Karppinen, Progress in Solid State Chemistry **43**, 1 (2015).
- [46] H. Kato, T. Okuda, Y. Okimoto, Y. Tomioka, K. Oikawa, T. Kamiyama, and Y. Tokura, Phys. Rev. B **69**, 184412 (2004).
- [47] A. Winkler, N. Narayanan, D. Mikhailova, K. G. Bramnik, H. Ehrenberg, H. Fuess, G. Vaitheeswaran, V. Kanchana, F. Wilhelm, A. Rogalev, A. Kolchinskaya, and L. Alff, New J. Phys. **11**, 073047 (2009).
- [48] C. M. Thompson, J. P. Carlo, R. Flacau, T. Aharen, I. A. Leahy, J. R. Pollicemi, T. J. S. Munsie, T. Medina, G. M. Luke, J. Munevar, S. Cheung, T. Goko, Y. J. Uemura, and J. E. Greedan, J. Phys.: Condens. Matter **26**, 306003 (2014).

Supplementary information for: Spin-orbit coupling controlled ground state in $\text{Sr}_2\text{ScOsO}_6$

A. E. Taylor,¹ R. Morrow,² R. S. Fishman,³ S. Calder,¹ A.I. Kolesnikov,⁴

M. D. Lumsden,¹ P. M. Woodward,² and A. D. Christianson^{1,5}

¹Quantum Condensed Matter Division, Oak Ridge National Laboratory, Oak Ridge, Tennessee 37831, USA

²Department of Chemistry, The Ohio State University, Columbus, Ohio 43210-1185, USA

³Materials Science and Technology Division, Oak Ridge National Laboratory, Oak Ridge, Tennessee 37831, USA

⁴Chemical and Engineering Materials Division, Oak Ridge National Laboratory, Oak Ridge, Tennessee 37831, USA

⁵Department of Physics and Astronomy, The University of Tennessee, Knoxville, TN 37996, USA

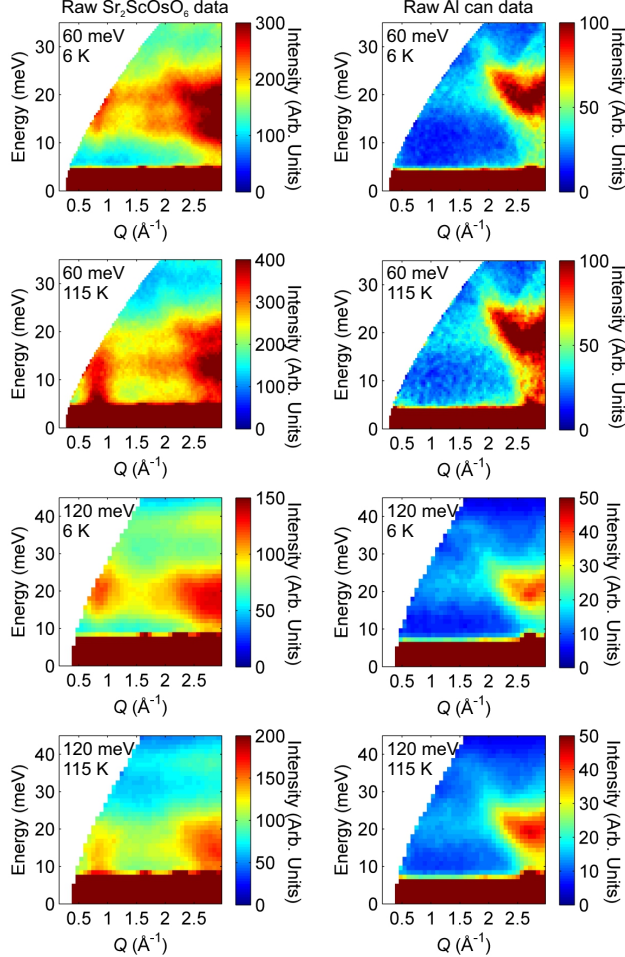


Figure S1. (Color online) Neutron scattering intensity maps showing the $\text{Sr}_2\text{ScOsO}_6$ data before Al can subtraction and the raw Al can data, as indicated. Labels on each plot indicate the temperature and incident energy used in the measurements.

INELASTIC NEUTRON SCATTERING

Here we present additional figures from the neutron scattering measurements on SEQUOIA. A closed-cycle refrigerator was used to access temperatures between 6 K and 115 K. Measurements were performed using incident

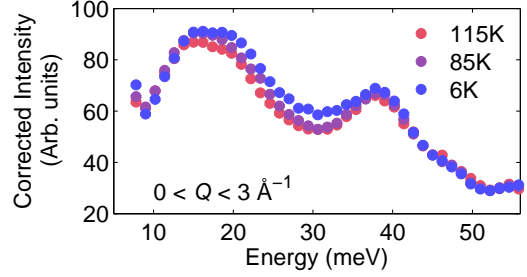


Figure S2. (Color online) Constant wavevector cuts averaged over a large low-Q range, 0 to 3 \AA^{-1} . Data are from the $E_i = 120 \text{ meV}$ SEQUOIA datasets measured on $\text{Sr}_2\text{ScOsO}_6$ with equivalent background measurements of the empty Al can subtracted. Data has been corrected for the Bose thermal population factor.

energies, E_i s, of 60 and 120 meV with chopper frequencies of 180 and 300 Hz, respectively. The sample was sealed in a 4 mm-thick flat-plate Al can, and an identical empty can was measured as a background. Empty Al-can measurements were subtracted from all the data sets presented in the main text. Figure S1 shows raw data collected from $\text{Sr}_2\text{ScOsO}_6$ prior to the empty can subtraction for temperatures above and below T_N . The equivalent raw data used for the empty can background subtraction are also shown, but presented on a lower intensity scale in order that features are visible. It is clear from comparing these intensity maps that the scattering attributed to magnetic fluctuations results from $\text{Sr}_2\text{ScOsO}_6$, and not a background feature.

In Fig. S2 we present constant wavevector cuts averaged over a large low-Q range, 0 to 3 \AA^{-1} , in order to include all magnetic scattering and enable us to compare data between different temperatures up to high energies. These data have been corrected for the Bose factor to enable this comparison. The opening of the gap pushes intensity to higher energies in 85 K and 6 K datasets, but the 6 K data appears to converge with the other temperatures at $E \approx 40 \text{ meV}$, which we identify as Γ in the main text. There is a phonon mode present at $E \approx 38 \text{ meV}$ but its position remains constant with temperature.

The $\chi''(Q, E)$ data presented in Fig. 3(b) was calculated as follows, similar to the method described in

Kermarrec *et al.* [11]. The integrated intensity of the $E_i = 60$ meV data between $5 < E < 9$ meV and $0.5 < Q < 1.2 \text{ \AA}^{-1}$ was found at each temperature, then the 6 K data is used as a background. The Bose factor correction is applied to the resulting data, and the highest temperature point is then used to scale the saturated intensity to 1.

SPIN-WAVE MODEL

In addition to the $J_2 \approx 0$ solution discussed in the main article, we attempted to find alternate $J_2 \neq 0$ solutions by searching a large region of parameter space. To include significant NNN interactions we allow both \mathcal{J}_1 and \mathcal{J}_2 to be anisotropic in spin space. We assume that both exchange interactions are unaffected by the weak monoclinic distortion, so all 6 NNN distances are equivalent. Therefore, the real-space alignment of the spins does not affect the calculation (although the spins are known to lie within the a - b plane [23]). As discussed in the article this is justified by the small distortion present in $\text{Sr}_2\text{ScOsO}_6$. Using the B - O - B' angles as a measure of distortion, the most-distorted (i.e. furthest from 180°) angle in $\text{Sr}_2\text{ScOsO}_6$ is $163.2(3)^\circ$ at 10 K [23]. Type I order is disrupted in $\text{La}_2\text{NaRuO}_6$ (which contains $\text{Ru}^{5+} 4d^3$ ions) giving an incommensurate magnetic ground state, but it has a least-distorted angle of 147.2° [6]. The approximate angle which induces significant changes for d^3 ions in DPs is indicated by the crossover from AFM $\text{Sr}_2\text{CrSbO}_6$ with angles of $166.6(5)$, $167(6)$ and $173(4)^\circ$, to FM interactions in $\text{Ca}_2\text{CrSbO}_6$ with angles $153.0(2)$, $151.9(2)$ and $152.5(2)^\circ$ [35] — although the spatial extent of the $3d$ orbitals will have impact on this result.

Therefore, we take the original NN hamiltonian, \mathcal{H}_{NN} , and we add the NNN term, giving

$$\begin{aligned}\mathcal{H} &= \mathcal{H}_{\text{NN}} - \sum_{\text{NNN}} \mathcal{J}_2^{\alpha\beta} S_{i\alpha} S_{j\beta} \\ &= \mathcal{H}_{\text{NN}} - \sum_{\text{NNN}} (J_2 \mathbf{S}_i \cdot \mathbf{S}_j + K_2 S_{ix} S_{jx})\end{aligned}$$

i.e. we have added a \mathcal{J}_2 similar to the \mathcal{J}_1 term discussed in the article. Explicitly the exchange interactions \mathcal{J}_1 and \mathcal{J}_2 are written as

$$\begin{aligned}\mathcal{J}_{1\alpha\beta} &= J_1 \delta_{\alpha\beta} + K_1 \delta_{\alpha x} \delta_{\beta x} \\ \mathcal{J}_{2\alpha\beta} &= J_2 \delta_{\alpha\beta} + K_2 \delta_{\alpha x} \delta_{\beta x}\end{aligned}$$

and $\alpha, \beta = \{x, y, z\}$.

To accurately search for solutions in the expanded parameter range, we introduce loose constraints on the parameter space. We solve for the four parameters J_1 , J_2 , K_1 , and K_2 based on four conditions as follows. First, the ground state of the Os spins is the type I AFM state depicted in Fig. 1(b) in the main text. To confirm the ground state, we minimize the classical energy, ϵ , among

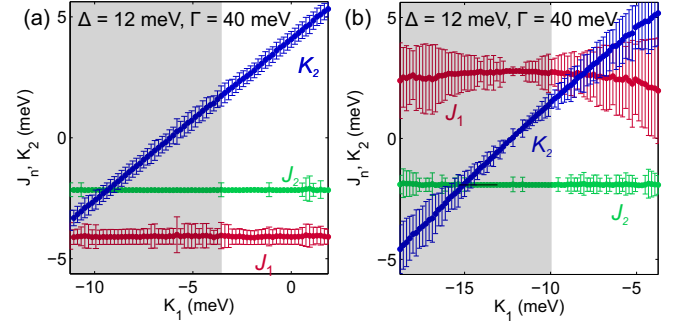


Figure S3. (Color online) Calculated parameters J_1 , J_2 , and K_2 as a function of K_1 , showing results for both branches of solutions that met the conditions described in the article. (a) shows results for which J_1 is antiferromagnetic, for which both J_1 and J_2 appear to be stable. Errorbars indicate the spread in each parameter calculated for each K_1 starting point, as described in the text.

the 64 different spin configurations with distinct Os spins aligned along the $\pm x$ directions in layers $z = 0, c/2, c$, and $3c/2$. Another stipulation for the local stability of the ground state is that the spin-wave frequencies are real throughout the magnetic Brillouin zone.

The second (third) condition is that the the bottom (top) of the spin-wave band is $\Delta = 12$ meV ($\Gamma = 40$ meV). We note that conditions two and three for Δ and Γ are not independent, and that exchange anisotropies K_1 and K_2 have the same effect on the spin dynamics as a single anisotropy term $\kappa = 3K_2 - 2K_1$. The conditions for the spin-wave energies Δ and Γ are closely satisfied. Finally, we apply a weak constraint using the T_N of 92 K. The expression for the mean-field (MF) transition temperature is $T_N = 2S(S+1)(3(J_2 + K_2) - 2(J_1 + K_1))/3$.

The parameters are calculated over a large range of K_1 values. We find ranges of possible solutions for J_1 , J_2 and K_2 for each K_1 , even though Δ and Γ depend only on the combination $\kappa = 3K_2 - 2K_1$, because the problem is under-determined. For different values of K_1 , we estimate the possible range of the other parameters by their spread for given starting points. This parameter spread occurs because the problem is under-determined, which helps to avoid arriving at a local minimum. Even with K_1 fixed, the coupled conditions for the stability of the ground state and for the spin-wave frequencies Δ and Γ are insufficient to completely determine the remaining three parameters. Although Δ and Γ depend only on the combination $\kappa = 3K_2 - 2K_1$, the ranges of solutions in J_1 and J_2 affect the range in K_2 for a fixed K_1 . For both branches, however, the average value for κ is constant over most of the range of K_1 , as seen in the linear relationship between K_1 and K_2 , Fig. S3. Note that ϵ does not simply depend on κ .

We find only two distinct branches of solutions, Fig. S3, one with $J_1 < 0$ (with $J_1 = -4.375$ meV, the value determined in the main article, consistent with this result) and

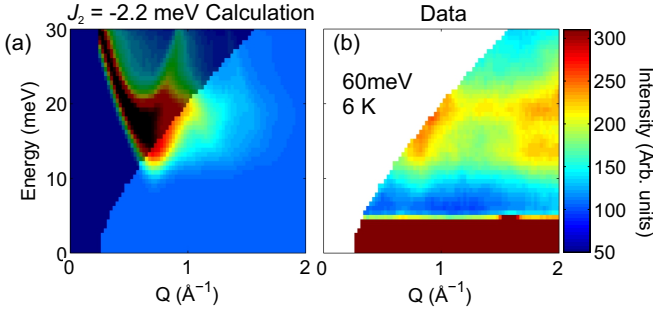


Figure S4. (Color online) Simulated powder-averaged spin-wave spectra for representative finite J_2 AFM solution with calculated parameters $K_1 = -3.0$, $J_1 = -4.13$, $J_2 = -2.2$, $K_2 = 2.2$ meV. This is compared to data collected at $T = 6$ K on SEQUOIA with $E_i = 60$ meV. The shaded region in the calculations indicates the region of (Q, E) space which is inaccessible in the experimental set-up.

the other with $J_1 > 0$. For both branches, the average value for κ is constant over the range of K_1 (Fig. S3), and the values of J_1 and J_2 are stable across the solutions. The grey regions show the solutions which are locally stable (have real spin wave solutions) but do not meet the classical condition for stabilizing the type I ground state, $(J_2 + K_2) > 0$ i.e. FM. Having determined the regions of parameter space which match our minimal constraints, we compare the simulated powder-averaged INS cross sections $S(Q, E)$ to the low-temperature data.

Figure S4 shows the results for J_1 antiferromagnetic for a representative solution, which qualitatively reproduces the 6 K data very well, similar to the $J_2 = 0$ solution. The results across the full range of K_1 are shown in the attached video D12_G40_AFM.mp4. The results with J_1 ferromagnetic do not reproduce the observed neutron scattering results, as shown for a representative parameter set in Fig. S5 and additionally over the entire range of parameters in the attached video D12_G40_FM.mp4. The Os^{5+} form factor from Ref. SM[1] was used for all simulations. The observation that solutions with antiferromagnetic J_1 provide a better description of the data than ferromagnetic J_1 is consistent with expectations considering the relevant NN exchange pathway, see Fig. 1(c). The direct overlap and Os-O-Os superexchange interactions are both expected to be AFM, as discussed in the main text.

The simulation presented in Fig. S4 are for parameters $K_1 = -3.0$ meV, $J_1 = -4.13$ meV, $J_2 = -2.2$ meV and $K_2 = 2.2$ meV. We choose $J_2 = -K_2$ as an interesting case, but the spin wave solutions that result are representative of the range of solutions presented in Fig. S3(a), as seen in the attached video D12_G40_AFM.mp4, because J_1 and J_2 are stable within the ranges $J_1 = -3.6$ to -4.7 meV and $J_2 = -1.8$ to 2.3 meV, and the combination $\kappa = 3K_2 - 2K_1$ is effectively tuning the size of the gap. Consider the particular solution where $J_2 = -K_2$,

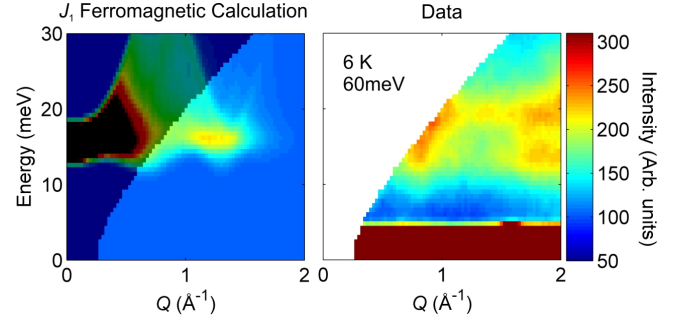


Figure S5. (Color online) Simulated powder-averaged spin-wave spectra for representative J_1 ferromagnetic solution with calculated parameters $K_1 = -5.6$, $J_1 = 2.4$, $J_2 = -1.9$, $K_2 = 4.3$ meV. This is compared to data collected at $T = 6$ K on SEQUOIA with $E_i = 60$ meV. The shaded region in the calculations indicates the region of (Q, E) space which is inaccessible in the experimental set-up.

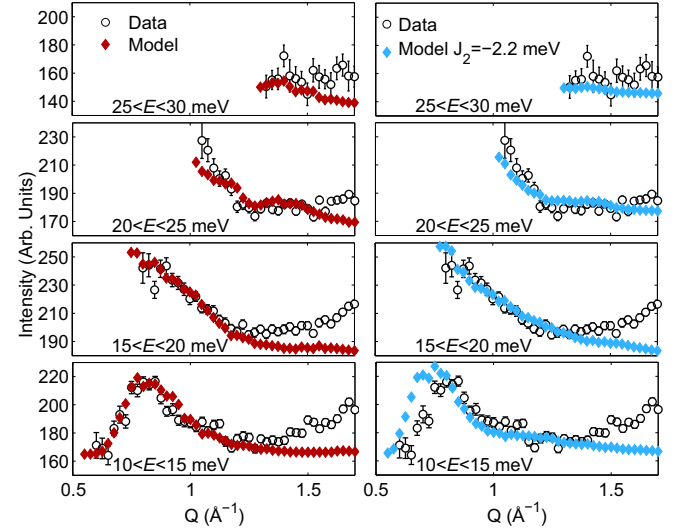


Figure S6. (Color online) Constant-energy cuts through the calculations (diamonds) and data (open circles), for $J_2 = 0$ model (LHS, red diamonds) and the model with $K_1 = -3.0$ meV, $J_1 = -4.13$ meV, $J_2 = -2.2$ meV and $K_2 = 2.2$ meV (RHS, blue diamonds). A global scale factor has been used for each calculation, and a flat background applied for each cut.

in this case the term in the Hamiltonian corresponding to the spin direction, x , cancels while the y and z components remain finite. This creates a subtle change in the calculated spin-wave spectrum as we will discuss. A range of solutions for $J_2 = -K_2$ are possible, with the exact solution $J_1 = -4.375$ meV and $K_1 = -3.75$ meV when $J_2 = -K_2 = 0$ with a mean-field $T_N = 181$ K. The $K_1 = -3.0$ meV, $J_1 = -4.13$ meV chosen here result from the mean-field stabilization of the ground state and the T_N constraint favoring solutions with slightly lower $T_N = 159$ K. Both T_N s are well within the expected range given the frustration in this system.

As the colormaps of the model with $J_2 \approx -2.2$ meV do not distinguish it from a model with $J_2 \approx 0$, we present constant-energy cuts through the data and each model in Fig. S6. The comparison shows that the non-zero y and z components in the Hamiltonian, $\mathcal{J}_{2yy} = \mathcal{J}_{2zz} \neq 0$, appear to have greatest influence on the spinwave spectrum at low energy, and here in the $10 < E < 15$ meV cut it is apparent that the $J_2 = 0$ model provides a much better description of the data. This is also a physically reasonable model in terms of relevant exchange pathways, as discussed in the main text.

As a check to the validity of our results, we also tried our calculations for different values of Γ and Δ . Here we show the calculated exchange parameters for $\Delta = 12$ meV and $\Gamma = 35$ meV, Fig. S7(a) and (b), and $\Delta = 8$ meV and $\Gamma = 40$ meV, Fig. S7(c) and (d). The resulting $S(Q, E)$ from all of these cases as shown in videos D12_G35_AFM.mp4, D12_G35_FM.mp4, D8_G40_AFM.mp4 and D8_G40_FM.mp4, and none of the parameters reproduce the data like the $\Delta = 12$ meV and $\Gamma = 40$ meV results.

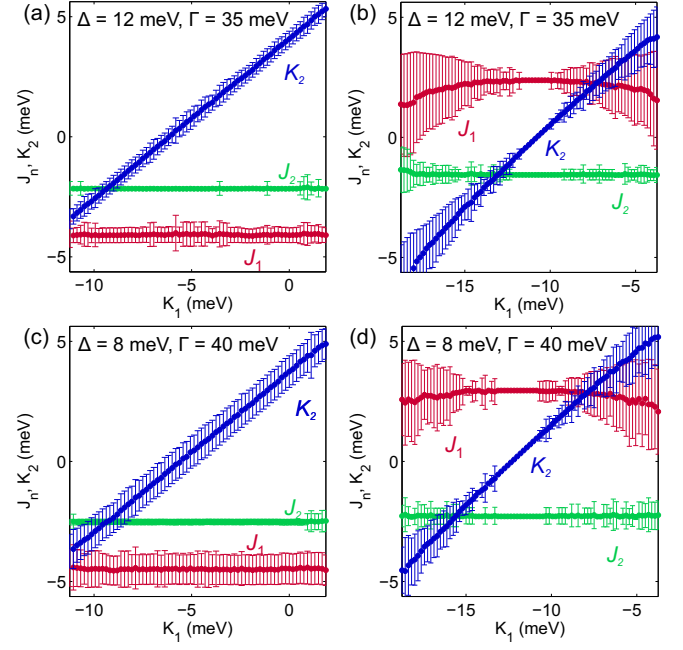


Figure S7. (Color online) Calculated parameters J_1 , J_2 , and K_2 as a function of K_1 , for alternative values of Γ ((a) and (b)) and Δ ((c) and (d)) showing results for both branches of solutions. Again the errorbars indicate the spread in each parameter calculated for each K_1 starting point, as described in the text.

-
- [1] K. Kobayashi, T. Nagao, and M. Ito, Acta Crystallographica Section A Foundations of Crystallography **67**, 473 (2011).